

Direct Numerical Simulations of Low- Rm MHD turbulence based on the least dissipative modes

ALBAN POTHÉRAT and VITALI DYMKOU

Applied Mathematics Research Centre,
Coventry University, Priory street Coventry CV1 5FB, United Kingdom

February the 8th, 2010

Abstract

We present a new spectral method for the Direct Numerical Simulation of Magnetohydrodynamic turbulence at low Magnetic Reynolds number. The originality of our approach is that instead of using traditional bases of functions, it relies on the basis of eigenmodes of the dissipation operator, which represents viscous and Joule dissipation. We apply this idea to the simple case of a periodic domain in the three directions of space, with an homogeneous magnetic field in the \mathbf{e}_z direction. The basis is then still as subset of the Fourier space, but ordered by growing linear decay rate $|\lambda|$ (*i.e* according to the *least dissipative modes*). We show that because the lines of constant energy tend to follow those of constant $|\lambda|$ in the Fourier space, the scaling for the the smallest scales $|\lambda^{\max}|$ in a forced flow can be expressed using this single parameter, as a function of the Reynolds number as $\sqrt{|\lambda^{\max}|}/(2\pi k_f) \simeq 0.5Re^{1/2}$, where k_f is the forcing wavelength, or as a function of the Grashof number G_f , which gives a non-dimensional measure of the forcing, as $|\lambda^{\max}|^{1/2}/(2\pi k_f) \simeq 0.47G_f^{0.20}$. This scaling is also found consistent with heuristic scalings derived by Alemany *et al.* (1979) and Pothérat & Albuoussière (2003) for interaction parameter $S \gtrsim 1$, and which we are able to numerically quantify as $k_{\perp}^{\max}/k_f \simeq 0.5Re^{1/2}$ and $k_z^{\max}/k_f \simeq 0.8k_f Re/Ha$. Finally, we show that the set of least dissipative modes gives a relevant prediction for the scale of the first three-dimensional structure to appear in a forced, initially two-dimensional turbulent flow. This completes our numerical demonstration that the least dissipative modes can be used to simulate both two- and three-dimensional low- Rm MHD flows.

1 Introduction

Turbulence can be described as a flow where a large number of different patterns evolve in complex interaction with one another. The knowledge of how much energy each of them carries at a given time then provides a reasonably simple statistical representation of the flow. Our purpose is to apply this very idea to turbulence in liquid metal flows subjected to an homogeneous external magnetic field, by tailoring existing spectral methods to this particular problem.

Although simple, these ideas express quite closely the phenomenology behind Kolmogorov (1941)'s famous theory of homogeneous isotropic turbulence. Here, the patterns are isotropic vortices sorted in three categories, according to their size l_k (or wavelength k): the large scales where energy is injected in the flow through some unspecified forcing, the inertial range, where mid size vortices pass on energy to smaller scales and the smallest scales of size $k_{\kappa} \sim Re^{3/4}$ where kinematic energy is dissipated by viscous friction ($Re = UL/\nu$ stands for the Reynolds number built on velocity U and length L , that are typical of the large scales, as well as the fluid kinematic viscosity ν). This

early picture has been a lot further refined since then, to account for more complex effects such as intermittency (see Frisch (1995) or Davidson (2004) for an overview).

The description of the flow in terms of patterns is also well reflected in the more mathematical spectral approach of turbulence, in which the solution is sought as a decomposition over the elements \mathbf{u}_i of a basis that spans the functional space it evolves in:

$$\mathbf{u} = \sum_i c_i(t) \mathbf{u}_i(\mathbf{x}). \quad (1)$$

The spatial dependence (\mathbf{x}) representing the flow patterns is carried by \mathbf{u}_i while the time dependence (t) appears in the coefficients of the expansion c_i only, so when (1) is injected into the set of Partial Differential Equations that governs the problem, the latter reduces to a simpler system of Ordinary Differential Equations (see Canuto *et al.* (2006) for a detailed account of spectral methods in fluid mechanics). Apart from clear advantages in terms of simplicity and precision, spectral methods can also be tailored to the physical reality they describe by choosing a basis (\mathbf{u}_i) that represents realistic flow patterns. This basis can be obtained from the set of eigenvectors and adjoint eigenvectors of the operator derived from the linear part of the motion equations, with the boundary conditions of the problem. In incompressible homogeneous turbulence in a spatially periodic domain, the corresponding operator is the self-adjoint Stokes operator. Its eigenvectors are Fourier functions (Constantin *et al.* (1985)), which are classically related to vortices of wavevector \mathbf{k} . When the flow is isotropic, vortices of all shapes are present in statistically equal number, so they are only sorted according to their size $\|\mathbf{k}\|$, which facilitates the direct comparison with Kolmogorov's phenomenology.

The picture is quite different for turbulence in liquid metals, where the application of a strong magnetic field \mathbf{B} breaks isotropy. The fluid motion induces eddy currents that produce strong Joule dissipation and interact with the magnetic field to yield the Lorentz force. When the magnetic Reynolds number Rm is small, as in most experiments at the laboratory scale, the magnetic field induced in turn by these currents can be neglected so the total magnetic field is externally imposed and not altered by the fluid motion. In the frame of this so-called Low Rm approximation (see Roberts (1967)), the Lorentz force mainly damps velocity variations along the magnetic field lines so vortices tend to be elongated in this direction, resulting in a strongly anisotropic flow. This effect is counteracted by inertial effects that tend to break up long vortices and promote isotropy in the flow. Just how isotropic the flow is, is determined by the ratio between the Lorentz force and inertia, expressed by the interaction parameter $S = \sigma B^2 L / (\rho U)$, where σ and ρ are the fluid's electric conductivity and density. For large S , in a three-dimensional cubic periodic domain, when all vortices extend from one boundary to the other, the flow is perfectly two-dimensional, so a transition exists between two- and three-dimensional turbulence. These effects were pointed out in the 1960's (Moffatt (1967)) while Sommeria & Moreau (1982) analysed the conditions for a channel flow perpendicular to the magnetic field \mathbf{B} to be quasi two-dimensional. More recently, Davidson (1997) explained how vortices evolve using the conservation of angular momentum.

Spectral methods have been numerically implemented to study this type of flow in three-dimensional periodic domains in several important pieces of work, starting with Schumann (1976) who showed that the free decay of initially isotropic turbulence under the influence of an homogeneous magnetic field in a three-dimensional periodic box at high S could lead to a two-dimensional state. Zikanov & Thess (1998) found that initially isotropic MHD flows held steady on average by application of a forcing localised in a spherical shell of the Fourier space exhibited intermittent shifts between two and three-dimensional states for $S \sim 1$. Intermittency was also observed by Thess & Zikanov (2007) in both forced and decaying MHD flows in a tri-axial ellipsoid. Most of these studies, however, have used the basis derived from the Stokes operator, and analysed the flow in terms of the modulus of the structure's wavevector k , when clearly, anisotropy imposes

that vortices of same k but oriented along or across the magnetic field should undergo very different levels of Joule dissipation and eventually carry very different levels of energy. Also, since no clear MHD equivalent to the Kolmogorov laws had been derived at the time, Kolmogorov laws themselves were used to impose a global cutoff frequency on k when once again, the resolution required to resolve the flow completely would be expected to decrease when spanning directions from across to along the magnetic field direction. Therefore, determining a more "MHD-suitable" basis, and obtaining MHD equivalent to the Kolmogorov laws for the dissipative scales in both two- and three-dimensional MHD forced turbulence are the precise questions we wish to address in this work, by going back to the initial idea of using a basis of functions that imitates flow patterns as closely as possible. We focus our attention on the configuration of a cubic domain, periodic in the three spatial directions, with an homogeneous magnetic field in the z direction. Although physically not realistic, these assumptions offer a simple but still meaningful test case for the application of our ideas, keeping in mind that results more directly comparable to experiments will have to come out of a configuration where boundaries that intercept the magnetic field lines at least, will be physical walls.

In the frame of the low Rm approximation, the Lorentz force appears as a linear term in the Navier-Stokes equation so the linear part of the latter is in fact the sum of the Stokes operator and that related to the Lorentz force (see Roberts (1967)). We have previously solved the spectral problem for this operator (Pothérat & Alboussière (2003)), shown that it was self-adjoint and that its sequence of eigenfunctions (the *least dissipative modes*) was able to finely mimic the anisotropic properties of MHD turbulence. We also showed that this sequence of modes achieved an upper bound for the attractor dimension of the system that was consistent with estimates obtained heuristically for the size of the smallest scales. It is worth mentioning that the spectral analysis of the same operator, but in the case where the boundaries orthogonal to \mathbf{B} are physical walls leads to a sequence of eigenfunctions that exhibit the correct Hartmann boundary layer profile in the vicinity of these walls (see Pothérat & Alboussière (2006), and Moreau (1990) for a review of the theory of these layers). In the present work, we will therefore numerically implement our previously found basis in order to extract the relevant modes and determine the MHD equivalent of the Kolmogorov scales. In section 2, we first recall and complement the properties of the linear part of the Navier-Stokes equation found in Pothérat & Alboussière (2003). We then implement this basis in an existing spectral code and determine some Kolmogorov-like laws for the small scales in three-dimensional MHD flows which should serve as a criterion to resolve the flow completely in section 3. Since an essential property of MHD turbulence is that it can be two-dimensional or three-dimensional, we devote section 4 to testing whether DNS based on the least dissipative modes can reproduce this feature. This leads us to find out the lengthscale of vortices in which three-dimensionality first appears when the intensity of the forcing is increased in an initially two-dimensional flow.

2 Principle of DNS based on the least dissipative modes

2.1 Problem formulation

We consider an incompressible, conducting fluid (density ρ , electrical conductivity σ and kinematic viscosity ν) in a three-dimensional periodic cube Ω of size L_0 under imposed homogeneous and steady magnetic field Be_z . In the frame of the low- Rm approximation, the governing equations can be reduced to the closed system made of momentum and mass conservation, which involve the flow velocity $\mathbf{u}(\mathbf{x}, t)$ and pressure $p(\mathbf{x}, t)$ only (see Roberts (1967) and Sommeria & Moreau (1982)). A third equation deduced from electric current conservation and the Ohm's law can be used to reconstruct the electric potential and the electric current *a posteriori*. We shall, however,

only need here the equations for $\mathbf{u}(\mathbf{x}, t)$ and $p(\mathbf{x}, t)$. These can be written in non-dimensional form by choosing reference length L , time L^2/ν , velocity ν/L , pressure $\rho\nu^2/L^2$ and a dimensionless external force $\|\mathbf{f}\|/L^{3/2}$, where $\|\cdot\| = (\int |\cdot|^2 d\Omega)^{1/2}$ is the usual norm in $L_2(\Omega)$ space. The Navier Stokes equations are then written:

$$\begin{aligned} \frac{\partial}{\partial t} \mathbf{u}(\mathbf{x}, t) + (\mathbf{u} \cdot \nabla) \mathbf{u} + \nabla p &= \nabla^2 \mathbf{u} - Ha^2 \nabla^{-2} \frac{\partial^2 \mathbf{u}}{\partial z^2} + G \mathbf{f}(\mathbf{x}, t), \\ \nabla \cdot \mathbf{u} &= 0, \end{aligned} \quad (2)$$

where $Ha = LB \sqrt{\frac{\sigma}{\rho\nu}}$ is the Hartmann number while $G = \frac{L^{3/2}}{\nu^2} \|\mathbf{f}\|$ is the Grashof number, which represents the forcing normalised by viscous forces (as in Doering & Gibbons (1995)). Consequently, the solution of (2) is defined by the only two relevant control parameters Ha and G in (2). The choice of L is not straightforward as it is not imposed by the geometry. It is noteworthy that if it is set to $L = \frac{1}{B} \sqrt{\frac{\rho\nu}{\sigma}}$, then the governing equations depend on the single dimensionless parameter G/Ha^3 . This reference length however ignores the dynamics of the large scales present in the flow. One would instead expect a better suited reference length to follow the forcing scale to some extent. Since, however, the latter is not specified at this stage, we shall choose $L = L_0$, as it represents *de facto* the largest achievable scale in our problem, and denote Ha_0 , the Hartmann number built on L_0 . It is worth stressing that we shall not try to minimise or ignore the effect of the boundaries where periodic conditions are applied. In particular, we shall also analyse two-dimensional flows where structures extend across the whole domain in the z direction. Although clearly not experimentally achievable, this configuration has often been used as an interesting toy-model for the study of the transition between two-dimensional and three-dimensional flows (Nakauchi *et al.* (1992); Zikanov & Thess (1998); Thess & Zikanov (2007)). Therefore, contrarily to many previous studies of turbulence where periodic domains are used to represent a small volume taken out of an homogeneous flow, and where structures of the size of the domain should therefore be avoided, the conditions under which structures extend over the full domain along z will be of interest in this work. For this reason, the length L_0 will be a meaningful parameter of the problem, wherever such two-dimensional vortices are considered (in section 4).

Two further non-dimensional numbers can be defined that are traditionally used in MHD turbulence: the usual Reynolds number $Re = \frac{UL_{\text{int}}}{\nu}$, with integral length scale

$$L_{\text{int}} = \frac{\pi}{2\|\mathbf{u}\|^2} \int_0^\infty \|\mathbf{k}\|^{-1} E(k) dk \quad (3)$$

gives a measure of the intensity of turbulence (Here, \mathbf{k} is the three-dimensional wavevector that appears in the Fourier transform of \mathbf{u} , $E(k)$ is the spectral power density of all wavevectors of norm k and $U = (\int E dk)^{1/2}$ is a reference velocity). Also, the magnetic interaction parameter $S = \sigma B^2 L_0 / (\rho U)$ represents the ratio of the Lorentz force to inertia. In freely decaying turbulence where boundaries are ignored, taking U as a reference velocity from the initial velocity field and L_{int} as a reference length, S becomes the only non-dimensional parameter that governs the problems. In our case however, only G and Ha_0 are known *a priori*. In this sense, they are the control parameters for this problem.

The problem is fully defined by the addition of periodic boundary conditions

$$\begin{aligned} \mathbf{u}(x, y, z, t) &= \mathbf{u}(x + a, y, z, t) \\ &= \mathbf{u}(x, y + b, z, t) \\ &= \mathbf{u}(x, y, z + c, t), \quad a, b, c \in \mathbb{Z} \end{aligned} \quad (4)$$

and of the initial condition

$$\mathbf{u}(x, y, z, 0) = \mathbf{u}_i(x, y, z). \quad (5)$$

These, together with the mass conservation, which simply implies that \mathbf{u} is a solenoidal vector field, are taken into account by specifying that the solution \mathbf{u} is sought in the functional space V^2 , a solenoidal subspace of Hilbert space H^2 . Since the spectral method we wish to implement is derived from the spectral properties of governing equations, these ought to be written in abstract form, with help of the Helmholtz decomposition:

$$\frac{\partial}{\partial t} \mathbf{u} = D_{Ha_0} \mathbf{u} + B(\mathbf{u}, \mathbf{u}) + G\mathbf{f}, \quad (6)$$

$$\mathbf{u}|_{t=0} = \mathbf{u}_i.$$

Details of the mathematical framework can be found in Dymkou & Poth erat (2009). The advantage of this form is that it gathers the linear part of the equations into a single operator that operates in V^2 onto itself:

$$D_{Ha} = P \left(\nabla^2 - Ha^2 \nabla^{-2} \frac{\partial^2}{\partial z^2} \right) : V^2 \rightarrow V^2. \quad (7)$$

P denotes the orthogonal projection onto the subspace of solenoidal fields, and nonlinear terms are represented by the bilinear operator $B(\mathbf{u}, \mathbf{u}) = P(\mathbf{u} \cdot \nabla) \mathbf{u}$.

In the absence of magnetic field, $Ha_0 = 0$ and the system reduces to the usual Navier-Stokes equation. Periodic boundary conditions then ensure that the eigenfunctions of the Stokes operator form a basis of V^2 (Foias *et al.* (2001)). They can thus be used for the spectral decomposition in order to reduce the problem to a simpler system of ordinary differential equations. For $Ha_0 \neq 0$, the physical relevance of the linear part can be seen by noticing that the Lorentz force only appears in D_{Ha_0} . The spectral properties of this operator are therefore expected to express the mode-selecting dissipation that results from its action on the flow. This makes the set of eigenfunctions of D_{Ha_0} a good candidate for the choice of the basis of modes required in the solution's expansion (1). We have previously found these in (Poth erat & Alboussiere (2003)) and shown that they constituted a basis of V^2 , so we shall now summarise and extend these results derived from the spectral characteristics of the dissipation operator D_{Ha} .

2.2 Spectral properties of the D_{Ha} operator for any given Ha

D_{Ha} is a linear operator. The boundary conditions are accounted for in the definition of the domain of the operator, defined as $D(A) = V^2(\Omega)$. Since Ω is bounded, the natural injection of V^2 into $L_2(\Omega)$ is compact, thus D_{Ha} , as an operator in $L_2(\Omega)$, is compact (Foias *et al.* (2001)). Also, this operator is self-adjoint and therefore possesses a discrete set of eigenvalues ($\lambda_{\mathbf{k}}$) and eigenfunctions $\mathbf{v}^{\mathbf{k}}$ that form an orthonormal basis of the $L_2(\Omega)$ space. We have shown in Poth erat & Alboussiere (2003) that the eigenfunctions $\mathbf{v}^{\mathbf{k}} = (v_i^{\mathbf{k}})_{i \in \{x, y, z\}}$ are a subset of the usual Fourier space:

$$v_i^{\mathbf{k}} = V_i e^{j2\pi \mathbf{k} \cdot \mathbf{x}}, \quad (8)$$

with wavenumbers $\mathbf{k} = (k_x, k_y, k_z) \in \mathbb{Z}^3$, constants $V_i \in \mathbb{C}$ and where j is the imaginary unit. The corresponding eigenvalues are

$$\lambda_{\mathbf{k}} = -4\pi^2(k_x^2 + k_y^2 + k_z^2) - Ha^2 \frac{k_z^2}{k_x^2 + k_y^2 + k_z^2}. \quad (9)$$

We denote the set of all eigenvalues (9) by $\sigma_\infty(D_{Ha})$. Since $\lambda_{\mathbf{k}}$ represents the linear decay rate of mode $\mathbf{v}_{\mathbf{k}}$ by D_{Ha} , and $\lambda_{\mathbf{k}} < 0$, $(\lambda_{\mathbf{k}})$ and $v_{\mathbf{k}}$ can be arranged by growing dissipation. This singles out $\lambda_{\mathbf{k}}$ as a spectral parameter that naturally reflects the effects of the Lorentz force. From the definition (9), we see that for $Ha = 0$, $|\lambda_{\mathbf{k}}|/(2\pi)^2$ reduces to the square length $k^2 = \|\mathbf{k}\|^2$ of the wave vector \mathbf{k} which is the usual spectral parameter in non-MHD isotropic turbulence (see Figure1(a)). In the MHD case, different values of the magnetic field B or of the reference length L that enter the definition of Ha yield different sets of eigenvalues (see Figure1(a)-(d)). Such dependency is absent in the usual Fourier basis ordered by growing $\|\mathbf{k}\|$. The main novelty introduced by using this basis thus doesn't reside in the elements of the basis themselves but rather in the fact that they are ordered by growing values of $|\lambda_{\mathbf{k}}|$ instead of by growing k . This earns these modes their denomination of *least dissipative*. Furthermore, we previously showed (Pothérat & Alboussière (2003)) that the set of least dissipative modes required to describe the flow possessed the anisotropy properties predicted heuristically for such MHD flows. In the light of (9), the sequence $(-\lambda_{\mathbf{k}})^{1/2}/(2\pi)$ therefore appears as an anisotropic generalisation of the usual k -sequence, and the spectral decomposition (1) of \mathbf{u} can now be rewritten as

$$\mathbf{u}(\mathbf{x}, t) = \sum_{|\lambda_{\mathbf{k}}| < |\lambda^{\max}|} c_{\lambda_{\mathbf{k}}}(t) \mathbf{v}_{\lambda_{\mathbf{k}}}(\mathbf{x}), \quad (10)$$

where $c_{\mathbf{k}}(t)$ are the expansion coefficients, $\mathbf{v}_{\lambda_{\mathbf{k}}}(\mathbf{x})$ are the eigenvectors of D_{Ha} for eigenvalue $\lambda_{\mathbf{k}}$ and λ^{\max} defines the maximum resolution required to resolve the flow completely.

2.3 Choice of the set of least dissipative modes

At this point, we still lack two parameters to be able to choose the set of modes to fully resolve a given flow, defined by the values of G (or Re) and Ha_0 . Firstly, the 'shape' of the set of modes is determined by the value of Ha only. We have however defined Ha_0 using the domain size L_0 , as a reference length. Clearly, for Ha to reflect the actual physics of the flow, another reference length L should be found that accounts for the forcing scale in one way or another. Secondly, the number of modes N required to fully resolve the flow or, equivalently, the largest value of $|\lambda|$, $|\lambda^{\max}|$ in (10) must be determined in such a way that the flow is fully represented by its projection onto the set of N least dissipative modes defined by $|\lambda| < |\lambda(N)| = |\lambda^{\max}|$. For this, the global attractor of the motion equations has to be entirely included in the functional subspace spanned by the N least dissipative modes. Consequently, if d_M is the dimension of this attractor, or equivalently the number of degrees of freedom of the flow, we must have $|\lambda^{\max}| \geq |\lambda(d_M)|$. Unfortunately, it is difficult to obtain a precise estimate for d_M . Its physical interpretation, however, can be easily understood: in both the non-MHD and the MHD case, the reason why d_M is finite is that viscous dissipation introduces a cutoff at the small scales, beyond which flow structures carry a vanishingly small amount of energy. Constantin *et al.* (1985) give an elegant illustration of the physical meaning of these mathematical concepts. This cutoff wavelength can be estimated heuristically, which, in turn leads to scalings for N . The most famous example is that of the three-dimensional non-MHD case, where the heuristic Kolmogorov scale $k^{\max} = k_\kappa \simeq C_\kappa Re^{3/4}$ ($= |\lambda^{\max}|^{1/2}/2\pi$ in our notations, and where $C_\kappa > 1$, Kolmogorov (1941)) gives an estimate that is precise enough to be used as a criterion to fix the number of determining modes as $N \simeq C_\kappa^3 Re^{9/4}$ in a Fourier-based DNS. In two-dimensional turbulence, a precise estimate for the attractor dimension (Doering & Gibbons (1995)) and a heuristic scaling for the size of the smallest, or *Kraichnan scales*, (Kraichnan (1967); Ohkitani (1989)) coincide precisely with $k^{\max} = k_\kappa \simeq G^{1/3}(1 + \log G)^{1/6}$ where $k^{\max} = |\lambda^{\max}|^{1/2}/2\pi$.

In the MHD case, viscous dissipation still determines the cutoff scale, even though Joule dissipation extracts energy at all scales. Alemany *et al.* (1979) and Pothérat & Alboussière (2003) used this

idea, further assumed that the anisotropy k_\perp/k_z was scale-independent and that inertia balanced the Lorentz force at all scales to derive some heuristic scalings for the cutoff value λ^{\max} and N , when $S \gtrsim 1$:

$$N \simeq C_0 \frac{Re^2}{Ha}, \quad (11)$$

$$\frac{\sqrt{|\lambda^{\max}|}}{2\pi k_f} \simeq C_\lambda Re^{1/2}. \quad (12)$$

We have here expressed λ^{\max} with respect to the largest forcing scale in the problem $L_f = L_0/k_f$ to reflect the fact that for spatially periodic domains, the forcing scale is a relevant large scale that determines the small scales while the size of the computational domain isn't. Since the set of least dissipative modes is a subset of that of Fourier modes, these scalings can be more classically expressed in terms of the smallest scales across (subscript \perp) and along the magnetic field by virtue of the properties of (9):

$$\frac{k_z^{\max}}{k_f} \simeq \pi k_f C_\lambda^2 \frac{Re}{Ha}, \quad \frac{k_\perp^{\max}}{k_f} \simeq C_\lambda Re^{1/2}. \quad (13)$$

We have been able to partly confirm these scalings by finding an upper bound for the attractor dimension (Pothérat & Alboussière (2003)). C_0 or C_λ however remain to be evaluated, so no practical criterion currently exists for the number of determining modes in flows where a magnetic field is present. The next section is therefore devoted to searching numerically the values of L and λ^{\max} . In particular, we shall estimate the lowest values of C_λ for which the flow is fully resolved for $S \gtrsim 1$. When $S \gg 1$, the flow becomes two-dimensional so the set of least dissipative modes becomes the two-dimensional isotropic set of Fourier modes defined by $N \gtrsim k_k^2$ (or $\lambda^{\max} = (2\pi k_k)^2$). When $S \ll 1$, the effects of the Lorentz force become small and the set of least dissipative modes differs little from that of the usual three-dimensional isotropic set of Fourier modes $N \simeq C_\kappa^3 Re^{9/4}$ (or $\lambda^{\max} = (2\pi k_\kappa)^2$).

At this point, it is important to notice that a flow described by the set of least dissipative modes with λ^{\max} determined by the rules above is resolved exactly, without any approximation, as all energy and dissipation containing modes are contained in the attractor. In particular, a clear distinction should be made between solving the equations by projection on the full set of least dissipative modes, which is a type of Direct Numerical Simulation, and approaches such as Large Eddy Simulations where part of the spectrum is modelled and not resolved. Both approaches could even be combined to achieve important reductions in computational cost.

3 Determination of the exact set of modes required to resolve the flow for $S \gtrsim 1$

3.1 Numerical system and procedure

We base our DNS on the eigenfunctions of the dissipation operator. Since these are a subset of the usual Fourier modes, we use the code developed by Knaepen & Moin (2004) and Vorobev *et al.* (2005) where the problem formulated in section 2.1 was implemented and fully tested. It relies on traditional spectral methods based on a Fourier decomposition, with Fast Fourier Transform and a fourth-order low-storage time-integration Runge-Kutta scheme (see Rogallo (1981) and Williamson (1980)). The alias error resulting from the bilinear products is removed by phase-shifting method (Rogallo (1981); Orszag & Patterson (1971)), which allows us to retain all of the Fourier modes but requires eight evaluations during each time step. We adapt this code to our needs of performing

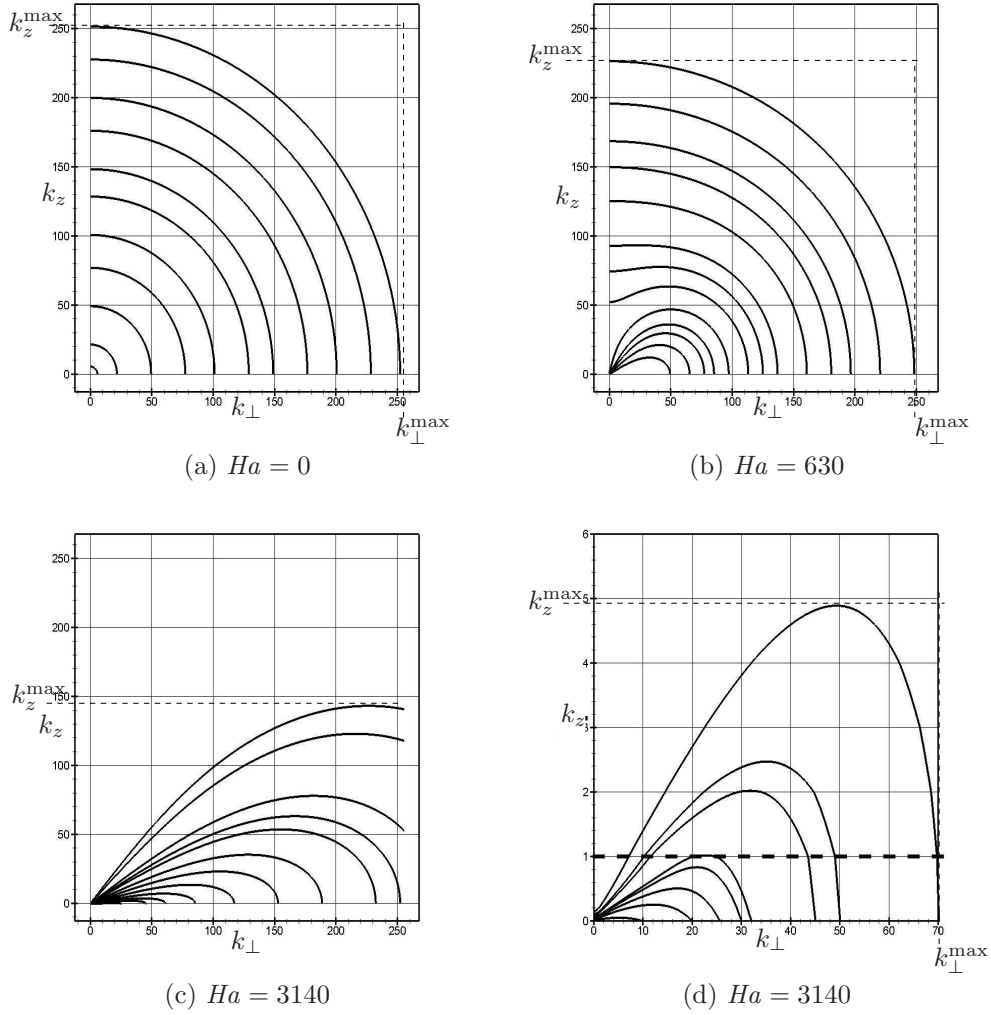


Figure 1: Iso- λ curves for different values of Ha . Note that all families of curves (except those for $Ha = 0$) can be scaled down to a single family in the $(k_{\perp}/Ha, k_z/Ha)$

plane where $k_{\perp} = \sqrt{k_x^2 + k_y^2}$. Values of k_{\perp}^{\max} and k_z^{\max} are marked on arbitrary iso- λ curves to illustrate how they are related to λ^{\max} .

calculations using set of modes that satisfy $|\lambda_{\mathbf{k}}| < |\lambda^{\max}|$, simply by setting unneeded modes to zero when required. In all calculations presented in the whole of section 3, initial velocities are set to zero ($\mathbf{u}(t=0) = 0$). The flow is driven by two distinct types of constant forcing \mathbf{f} in (6), that respectively favour two-dimensional and three-dimensional structures. The two-dimensional forcing is applied to Fourier modes with wavevectors $\mathbf{k}_{\mathbf{f}} = (k_{fx}, k_{fy}, k_{fz}) \in \{(6, 6, 0), (7, 7, 0), (9, 9, 0)\}$

$$\mathbf{f}_{2D}(\mathbf{x}, t) = \sum_{\mathbf{k}_{\mathbf{f}}} \left(\sin(k_{fx}2\pi x) \cos(k_{fy}2\pi y) \mathbf{e}_x + \cos(k_{fx}2\pi x) \sin(k_{fy}2\pi y) \mathbf{e}_y \right), \quad (14)$$

and tends to generate a flow with no velocity component nor velocity variations in the z -direction. Since the numerical algorithm would not otherwise allow the solution of the problem to be three-dimensional at all, we add a small constant force of amplitude $\varepsilon = 10^{-3}$ (relative to \mathbf{f}) in each ball $\|\mathbf{k} - \mathbf{k}_{\mathbf{f}}\| < 2$. There are several other reasons for this choice: firstly, the forcing has to be a combination of the set of modes used for the expansion. In this regard, a practically z -independent forcing can be used to simulate both two-dimensional flows (for which the effect of the small three-dimensional component of the forcing falls within the numerical error) and three-dimensional flows. The second reason is that this type of constant weakly three-dimensional forcing strongly resembles that obtained in liquid metal experiments by injecting electric current through metallic electrodes embedded in insulating Hartmann walls (Sommeria (1986), Sommeria (1988), Delannoy *et al.* (1999)). Our most recent experiments on electrically driven channel flows under transverse magnetic fields (Klein *et al.* (2009); Klein & Pothérat (2010)) have indeed confirmed the previous theoretical prediction that in such experiments, even for high values of Ha , inertia induced some slight velocity variations along the magnetic field lines, so that three-dimensional vortex instabilities such as those analysed by Thess & Zikanov (2007) do not occur in strictly two-dimensional, or even strictly quasi two-dimensional flows, but rather is some weakly three-dimensional flow (Pothérat *et al.* (2000)), which our weakly three-dimensional forcing imitates. Finally, Vorobev *et al.* (2005) have suggested that the two or three-dimensional nature of the forcing had no noticeable influence on the anisotropy of intermediate and small scales. This is supported by the properties of the least dissipative modes, as they imply that the small scales are determined by G , which only carries the intensity and the scale of the forcing, and Ha (Pothérat & Alboussière (2003)). To check this point further, we have performed a series of computations in the same conditions as those described above, but with a three-dimensional forcing. The latter was chosen of the ABC type (Mininni *et al.* (2006)) so as to act on the three components of the velocity, and expressed as:

$$\begin{aligned} \mathbf{f}_{3D}(\mathbf{x}, t) = & (\cos(k_{fy}y) + 1.1 \sin(k_{fz}z)) \mathbf{e}_x + (1.1 \cos(k_{fz}z) + 0.9 \sin(k_{fx}x)) \mathbf{e}_y \\ & + (0.9 \cos(k_{fx}x) + \sin(k_{fy}y)) \mathbf{e}_z \quad \text{with } \mathbf{k}_{\mathbf{f}} = (6, 6, 6). \end{aligned} \quad (15)$$

All calculated cases are summarised in table 1.

3.2 Determination of the length scale L_{opt}

We first address the problem of choosing the best suited reference length L that enters the definition of the Hartmann number Ha , for a flow at given Ha_0 and G (or Re). This problem appears only in three-dimensional flows as in two-dimensional flows, the least dissipative modes reduce to the isotropic set of two-dimensional Fourier modes. At this point, one should remember that the choice of the basis is arbitrary and should not have any impact on the final solution, as long as its elements can be combined to obtain all the energy and dissipation-carrying modes. In the particular case of a basis of least dissipative Fourier modes, this gives us the freedom to leave L as a free parameter *a priori*, and to fix it so as to obtain a basis that contains the least possible non-energetic, non-dissipative modes, that are superfluous for the description of the solution. How this can be done

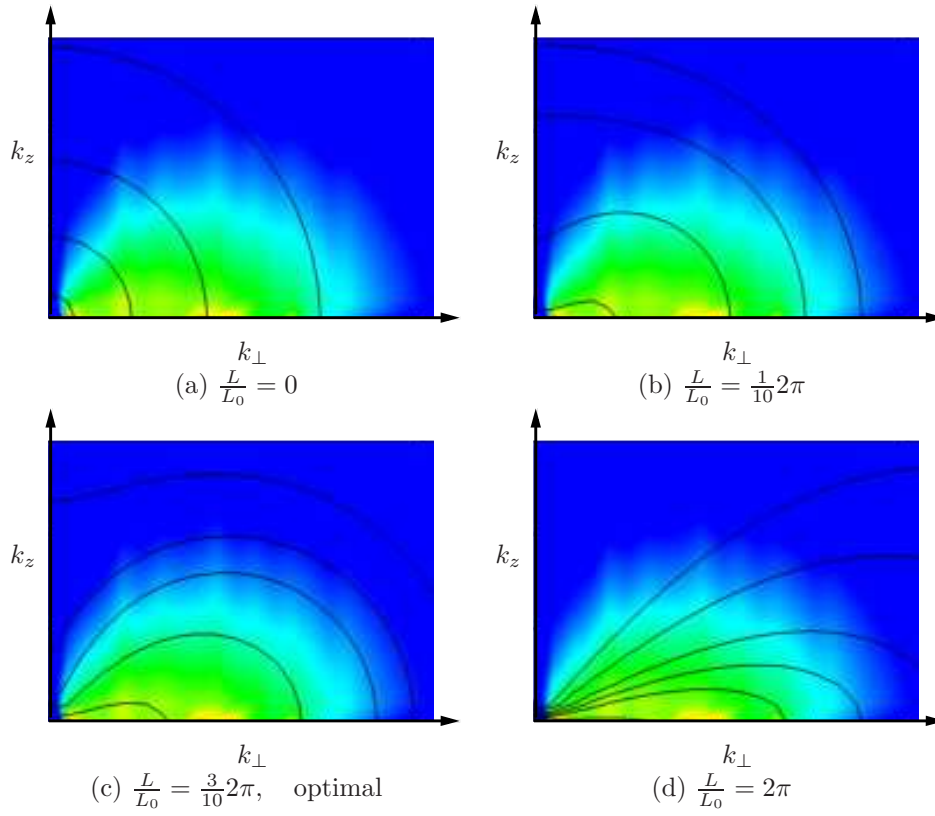


Figure 2: Contours of spectral density of energy $E(k_{\perp}, k_z)$ (colours) with iso- k and iso- λ curves (solid lines) for several values of L at $Ha_0 = 80$ and $G = 2.94 \times 10^7$.

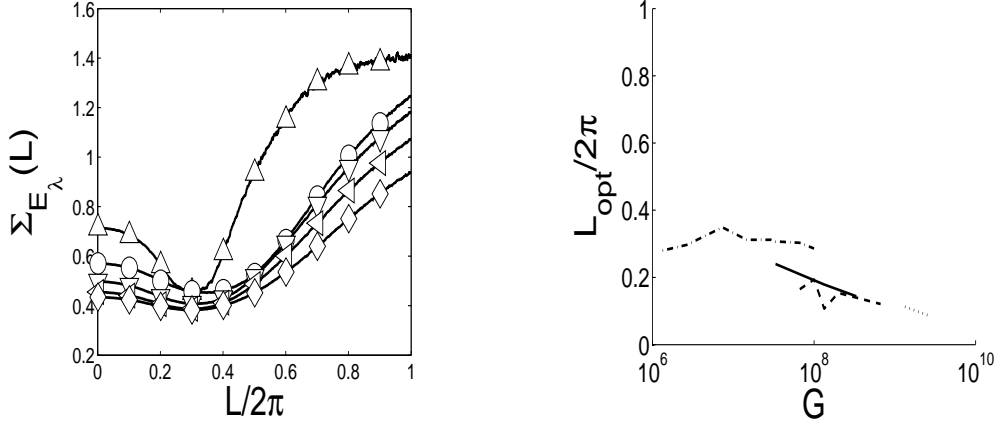


Figure 3: *Left:* Variations of $\Sigma_{E_\lambda}(L)$ for the cases listed in table 1. The minima indicate $L = L_{opt}$. Symbols are those from table 1. *Right:* variations of L_{opt} with Ha_0 and G for $Ha_0 = 80$ and 2D forcing (dash-dot), $Ha_0 = 400$ and 2D forcing (dashed), $Ha_0 = 1000$ and 2D forcing (dotted) and $Ha_0 = 400$ and 3D forcing (solid).

can be understood by analogy with the non-MHD case where the flow is expected to be isotropic in regions of the Fourier space located far enough from the forcing. There, the energy of a given mode \mathbf{k} is expected to depend on $\|\mathbf{k}\|$ only. Similarly, for the spectral parameter λ to be physically relevant to the MHD case we would expect each eigenmode of D_{Ha} of eigenvalue λ located far enough from the forced modes \mathbf{k}_f to carry approximately the same amount of energy. The erratic nature of turbulent flows, however, makes it impossible to satisfy this condition exactly, so we shall instead look for the optimal value L_{opt} of L that minimises the functional:

$$\Sigma_{E_\lambda}(L) = \sum_{v \in \sigma(D_{Ha})} \sum_{\mathbf{k}: \lambda(\mathbf{k})=v} \left| \frac{E_\lambda(\mathbf{k})}{E_\lambda} - 1 \right|, \quad (16)$$

where $\sigma(D_{Ha})$ refers to the finite set of eigenvalues of D_{Ha} for the numerical resolution considered, E_λ denotes the energy summed over all modes of eigenvalue λ and $E_\lambda(\mathbf{k})$ is the spectral energy density at point \mathbf{k} of the iso- λ surface. $\Sigma_{E_\lambda}(L)$ gives one possible overall measure of how strongly E varies over shells shaped according to the iso- λ surfaces in the Fourier space. In practice, we start from a "traditional" DNS resolved up to the Kolmogorov scale (these cases are gathered in table 1), and therefore over-resolved in the MHD case (on the basis that the attractor dimension decreases monotonically when Ha increases (Pothérat & Alboussière (2003))). This yields a reference solution from which $E(k_\perp, k_z)$ can be extracted. We then calculate the minimum of functional $\Sigma_{E_\lambda}(L)$ numerically (the variations of $\Sigma_{E_\lambda}(L)$ are shown on figure 3, left). This is illustrated on a typical example for $Ha_0 = 80$ and $G = 2.94 \times 10^7$ on figure 2 where the sets of iso- λ curves are plotted for several values of L along with the contours of $E(k_\perp, k_z)$. One sees that the iso- λ curves corresponding to $L_{opt}/L_0 = 0.3 \times 2\pi$ on Figure 2(c) follow the energy distribution well, as opposed to iso- \mathbf{k} lines, shown on Figure 2(a) that cross many different levels of energy. This shows that the basis of the least dissipative modes does carry the morphology of the energy distribution quite realistically, provided we choose $L \simeq L_{opt}$. It can be seen from the variations of L_{opt} with G for $Ha_0 \in \{80, 400\}$ on figure 3, that it depends little on either G or Ha_0 , around $0.3L_0 \times 2\pi$ for $Ha_0 = 80$ and $0.2L_0 \times 2\pi$ for $Ha_0 = 400$. The fact that it still varies a little with Ha_0 is certainly due in part to the "non-universality" introduced by the forcing, as the energy distribution clearly

Ha_0	G	$n_x \times n_y \times n_z$	Re	C_λ	C_κ	$\alpha_E(0.5)$	$Ha_{\text{opt}}/2\pi$	S_{opt}	symbol
2D forcing									
80	2.67×10^6	$064 \times 064 \times 064$	70	0.55	1.33	0.999	23.70	8.02	\triangle
80	7.34×10^7	$128 \times 128 \times 128$	97	0.81	2.07	0.996	27.80	7.97	\circ
80	1.47×10^7	$128 \times 128 \times 128$	159	0.63	1.43	0.998	24.80	3.87	∇
80	2.94×10^7	$128 \times 128 \times 128$	194	0.57	1.23	0.996	24.90	3.20	\triangleleft
80	3.34×10^7	$128 \times 128 \times 128$	195	0.57	1.23	0.995	24.50	3.08	\square
80	6.67×10^7	$128 \times 128 \times 128$	264	0.50	0.98	0.998	24.20	2.21	\diamond
400	6.67×10^7	$128 \times 128 \times 128$	216	0.71	1.13	0.995	65.80	20.04	\blacktriangle
400	1.00×10^8	$256 \times 256 \times 256$	245	1.11	2.07	0.986	77.40	24.45	\bullet
400	1.33×10^8	$128 \times 128 \times 128$	282	0.53	0.93	0.998	42.70	6.47	\blacktriangledown
400	2.00×10^8	$256 \times 256 \times 256$	343	0.90	1.61	0.994	61.40	10.99	\blacktriangleleft
400	6.67×10^8	$512 \times 512 \times 256$	575	1.28	1.09	0.986	48.25	4.05	\blacksquare
1000	1.33×10^9	$512 \times 512 \times 256$	935	1.08	1.52	0.998	112.70	13.58	\blacktriangle
1000	2.67×10^9	$512 \times 512 \times 512$	1140	0.94	1.3	0.996	86.00	6.44	\bullet
3D forcing									
400	1.5×10^8	$256 \times 256 \times 256$	465	0.71	1.28	1.000	95.00	19.41	\blacksquare
400	6.0×10^8	$256 \times 256 \times 256$	512	0.62	1.19	0.999	71.00	9.84	\blacktriangledown

Table 1: Summary of all cases calculated with initial condition $\mathbf{u}(t=0) = 0$: Grashof number G , embedding spectral resolution $n_x \times n_y \times n_z$, Reynolds number Re , resolution (C_λ and C_κ), fraction of the total energy α_{3D} contained in modes with lower $|\lambda|$ than the value given by (17), “optimal“ Hartmann number $Ha_{\text{opt}} = Ha_0(L_{\text{opt}}/L_0)$, and “optimal“ interaction parameter $S_{\text{opt}} = Ha_{\text{opt}}^2/(4\pi^2 Re)$.

departs from the iso- λ lines in the vicinity of the forced modes. At a given Re , or G , the influence of these modes increases with Ha_0 , as for higher Ha_0 , the energy tends to stay closer to the (k_x, k_y) plane, which brings the smallest scales closer to the forced modes \mathbf{k}_f . For the purpose of performing DNS based on the least dissipative modes, a precise determination of L_{opt} is however not necessary as energy and dissipation spectra $E(\lambda)$ and $D(\lambda)$ obtained with L departing by around $\pm 30\%$ from L_{opt} , using only modes in the region $|\lambda| < |\lambda^{\text{max}}|$ (where λ^{max} was fixed according to (16) derived in the next section) yielded no significant discrepancy with those obtained from calculations based on L_{opt} exactly. This robustness also confirms that as long as the iso- λ curves follow the contours of energy well enough in the vicinity of the small scales, then the set of Fourier modes determined by λ^{max} contains very few non-relevant modes. Also, since $Ha_{\text{opt}} = BL_{\text{opt}}\sqrt{\sigma/(\rho\nu)}$ gives the most physically relevant measure of the Lorentz force, we shall now prefer it to Ha_0 to express the laws for the small scales (12) and (13).

3.3 Scaling laws for λ^{max}

Having chosen $L = L_{\text{opt}}$, we have fixed a family of modes, indexed by the corresponding sequence of values of λ . We now need to know how many of these modes are required to resolve the flow fully, for given values of Ha_{opt} and G (or Re). A usable estimate for this number is obtained through a value for the numerical constant C_λ that appears in the scaling law for the smallest scales $\lambda^{\text{max}}(Ha_{\text{opt}}, Re)$ (12). To find it, we select four cases covering different values of Ha , G , two and three-dimensional forcing. In each case, we first calculate the established state with resolution up to the Kolmogorov scale k_κ (summarised in table 1). Since this case is over-resolved, it serves as a reference for the energy and dissipation distribution in the Fourier space. We then recalculate several times the same flow, but resolved up to $|\lambda|^{1/2} = |\lambda^{\text{cut}}|^{1/2} = C_\lambda Re^{1/2}$ with different values

of C_λ and compare the corresponding power and dissipation density spectra $E(\lambda)$ and $D(\lambda)$ to those obtained in the reference DNS resolved to the Kolmogorov scale. Finally, the impact of the reduction in resolution on time dependent-flows is assessed by applying the same procedure to the freely decaying flow that follows a shutdown of the forcing in the established regime in the reference case, at $t = t_{\text{decay}}$.

Figure 4 summarises all calculated cases along with resolution and embedding resolution. The latter is of no incidence on the solution but gives a measure of the reduction in computational cost incurred by using our “ λ -based” approach, and this, even though the spectral code we are using hasn’t been optimised for it.

The time-averaged energy distributions in the (k_\perp, k_z) -plane ($k_\perp = \sqrt{k_x^2 + k_y^2}$) show no visible discrepancy between the reference case and those for $C_\lambda \in [0.29, 0.59]$. This indicates that even with the lowest resolution, which uses up to 64 times less modes than the reference case, the energy distribution, and the flow anisotropy are still qualitatively well rendered. An inspection of the corresponding λ -based energy and dissipation spectra from figure 5 and 6 confirms and refines the picture: the small energy and dissipation pile-up that inevitably occurs at the high- λ end of the spectrum certainly remains confined there for all Ha for $C_\lambda \gtrsim 0.5$. It does, however tend to slightly spread towards the higher end of the spectrum for lower values of C_λ , particularly in the dissipation spectra and in the cases at lower Re . Even though it is only pronounced in the $Ha_0 = 80$ case, this propagation of error toward larger scales is a usual symptom of under-resolution, and can be more easily spotted on the dissipation spectra. This error on the dissipation is further revealed when the flow is freely decaying. For each of our four reference cases, we have calculated such flows starting from an initial state in the established regime resolved up to the Kolmogorov scale. In each case, the subsequent evolution of the flow without forcing was calculated several times from this same initial condition, for the same maximum resolutions as those used to calculate the established flows. The evolution was calculated over 20 Joules times, after which the flow had lost most of its energy. As for the dissipation spectra in the established state, it turns out that a discrepancy between reference case and cases resolved with $C_\lambda < 0.5$ is visible in the evolution of both the total energy and of the energy in the field direction. Cases resolved with $C_\lambda \gtrsim 0.5$, on the contrary, match the reference case to a great precision, both when the flow is established and freely decaying. As a matter of fact, the decay curves for $C_\lambda \gtrsim 0.5$ cannot be distinguished from those of the reference case on the graph.

To quantify the precision reached for a given value of $C_\lambda = \sqrt{|\lambda^{\text{max}}|/(4\pi^2 k_f^2 Re)}$ over a wider range of parameters than those of the 4 reference cases calculated above, we define a reduced spectral parameter normalised by scaling (12): $l = \sqrt{|\lambda|/(4\pi^2 k_f^2 Re)}$, such that for $l = C_\lambda$, $\lambda = \lambda^{\text{max}}$. We have calculated the variations of total energy $\Sigma_E(l)$ and dissipation $\Sigma_D(l)$ contained in the spectral subspace enclosed in the iso- λ curve for each value of $l \leq C_\lambda$ for a selection of cases resolved beyond $C_\lambda = 0.5$ (summarised in table 1, along with their resolution expressed in terms of C_λ and C_κ). The results are illustrated on figure 7. Firstly, it turns out that for a given value of l , the ratio $\alpha_E(l)$ of $\Sigma_E(l)$ to the total energy $\Sigma_E(C_\lambda)$ is constant for all calculated cases, regardless of the values of Ha , G and of the nature of the forcing (with, in particular, $\alpha_E(l = 0.5) \simeq 0.99$ no matter how high C_λ is, as shown in table 1). In other words, the precision attained for a given value of C_λ remains essentially constant when Ha and G are varied beyond their values in the four reference cases calculated above. This brings further confirmation of the validity of scaling laws (12), and of their independence of the nature of the forcing. Secondly, the variations of $\Sigma_E(l)$ and $\Sigma_D(l)$ also comfort us in the choice of $C_\lambda \simeq 0.5$ as the minimum cutoff scale for full resolutions: this value is indeed located at the beginning of a plateau where further increase of resolution hardly brings any variation in the total energy and dissipation of the solution. Smaller values of C_λ , on the other

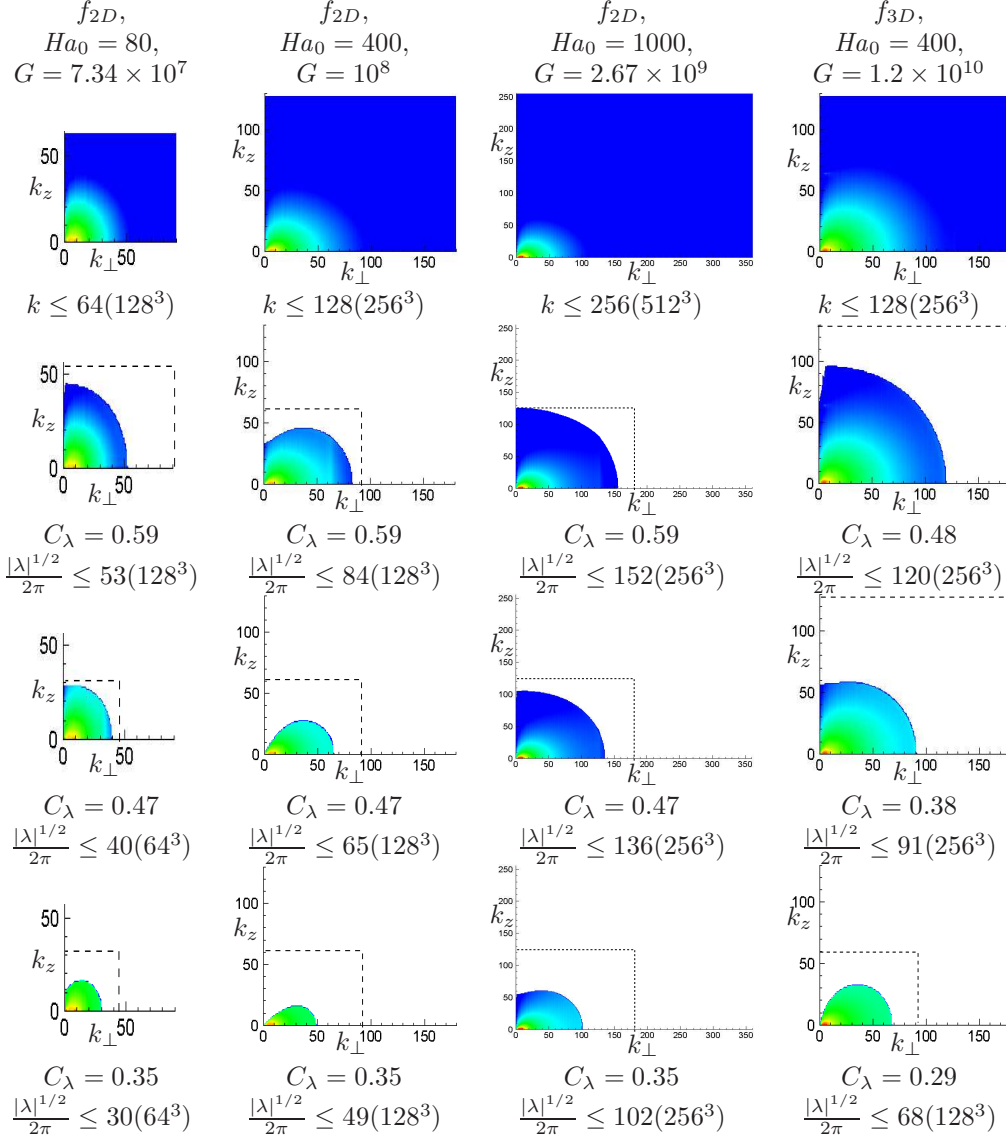


Figure 4: Logarithmic energy distribution in the (k_\perp, k_z) -plane. Blue dots correspond to low energy modes. Each column represents flows calculated with the same control parameters and the same forcing (indicated at the top), but with different resolutions, determined by the value of C_λ or, equivalently, by the spectral domain of resolution defined by $\lambda < \lambda^{\text{cut}}$, both indicated below each graph. Calculations from the first line are resolved up to the Kolmogorov scale $k_\kappa = C_\kappa Re^{3/4}$, with $Re = 97, 245, 1140, 512$ (see table 1). The dashed lines indicate the embedding resolutions used in our code (in brackets). Modes in the white area within this rectangular domain are set to 0.

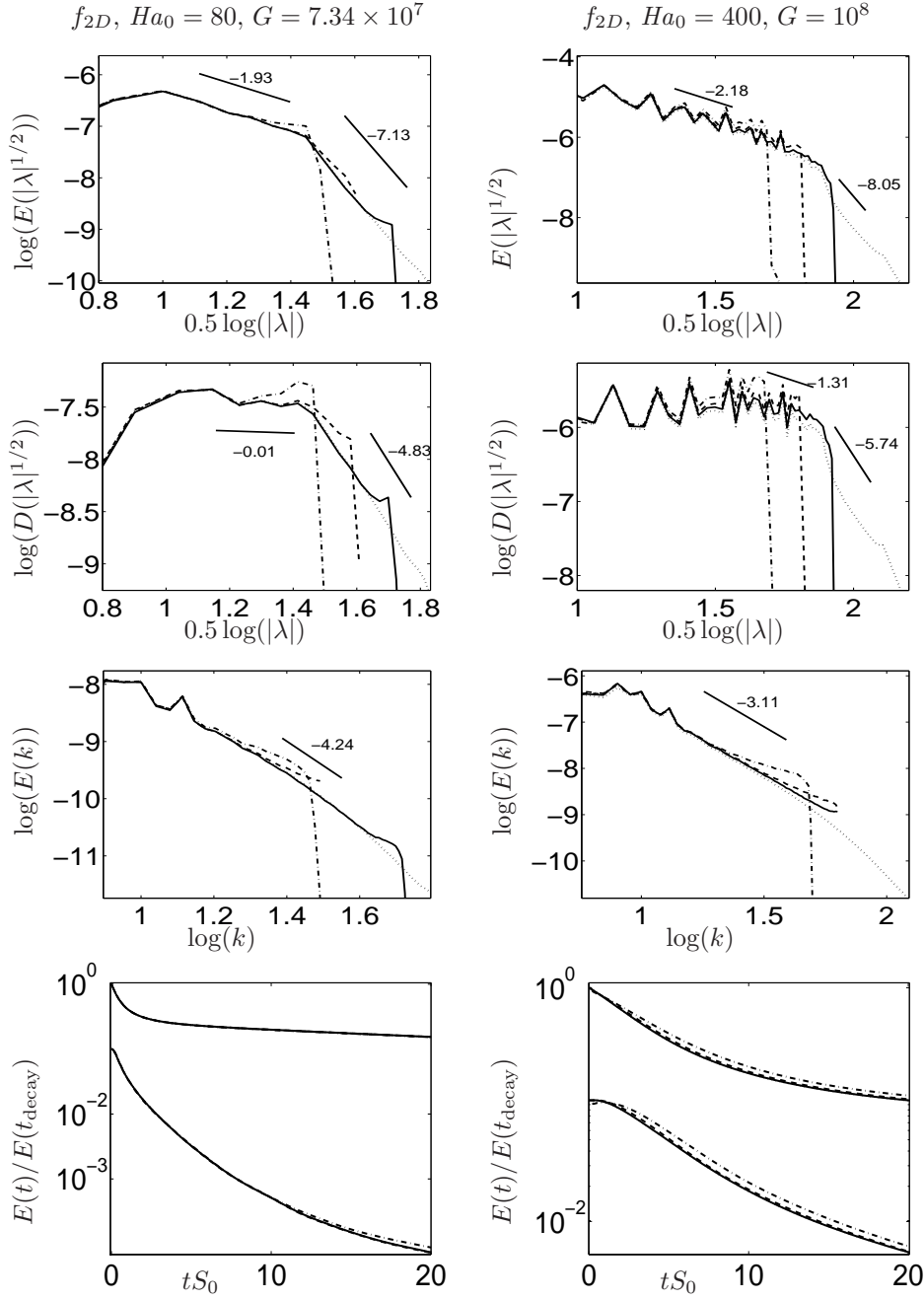


Figure 5: *Top*: energy density spectrum in λ -shells (statistically steady flow), *middle-top*: dissipation density spectrum in λ -shells (statistically steady), *middle-bottom*: energy density spectrum in k -shells (statistically steady), *bottom*: evolution of the total kinetic energy of freely decaying flows normalised by the total energy at the time when the forcing was shut down t_{decay} . For given Ha_0 and G , initial conditions are taken from the same statistically steady reference flow resolved up to the Kolmogorov scale for all values of λ^{cut} . Each column presents data from the corresponding cases from figure 4, from which different resolutions are represented by the following curves: *figure 5 left, right and figure 6 left*: $C_\lambda = 0.35$ (dash-dot), $C_\lambda = 0.47$ (dash), $C_\lambda = 0.59$ (solid), *figure 6 right*: $C_\lambda = 0.29$ (dash-dot), $C_\lambda = 0.38$ (dash), $C_\lambda = 0.48$ (solid). Dotted lines correspond to the reference case resolved up to the Kolmogorov scales $C_\kappa Re^{3/4}$.

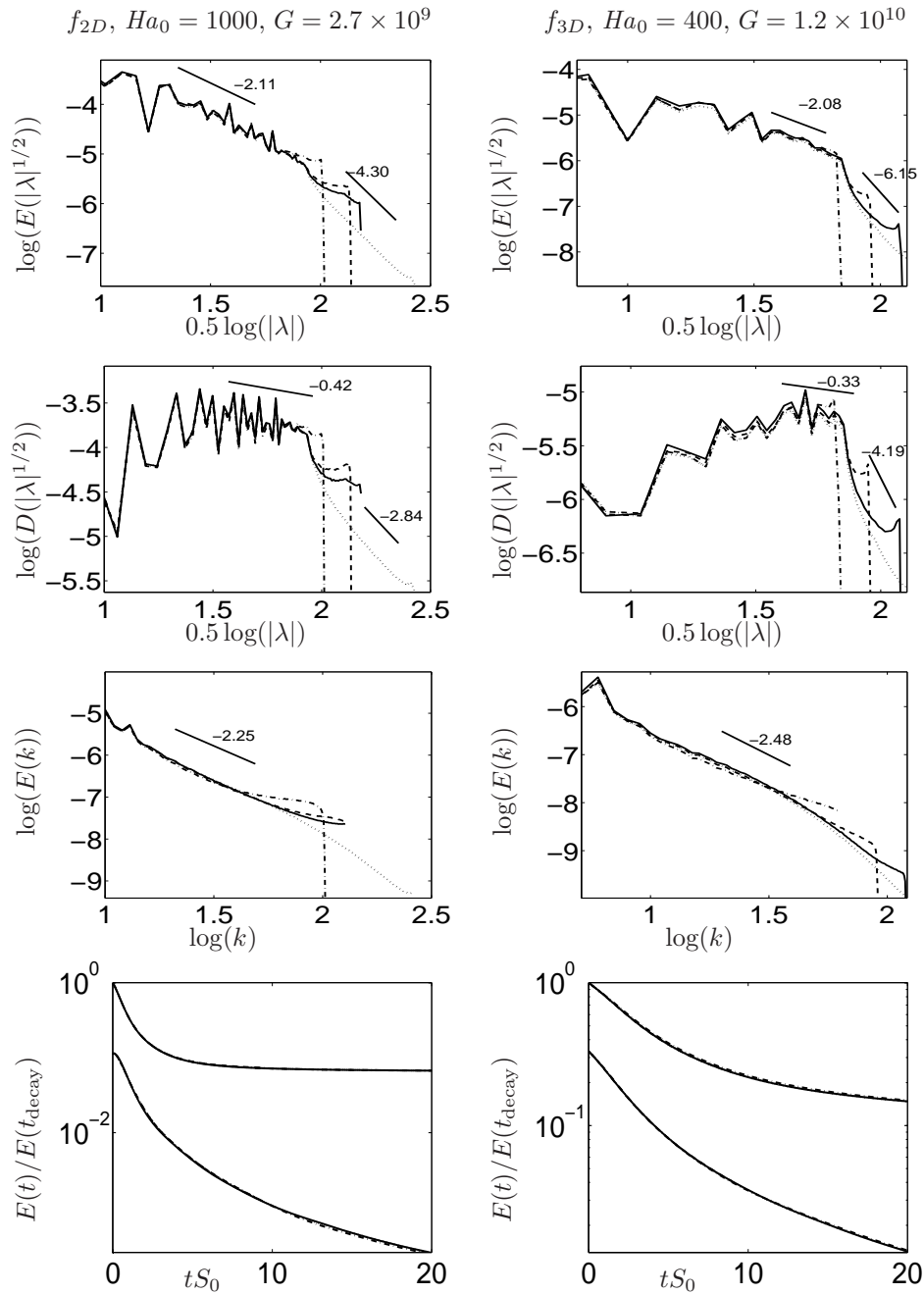


Figure 6: (figure 5 continued)

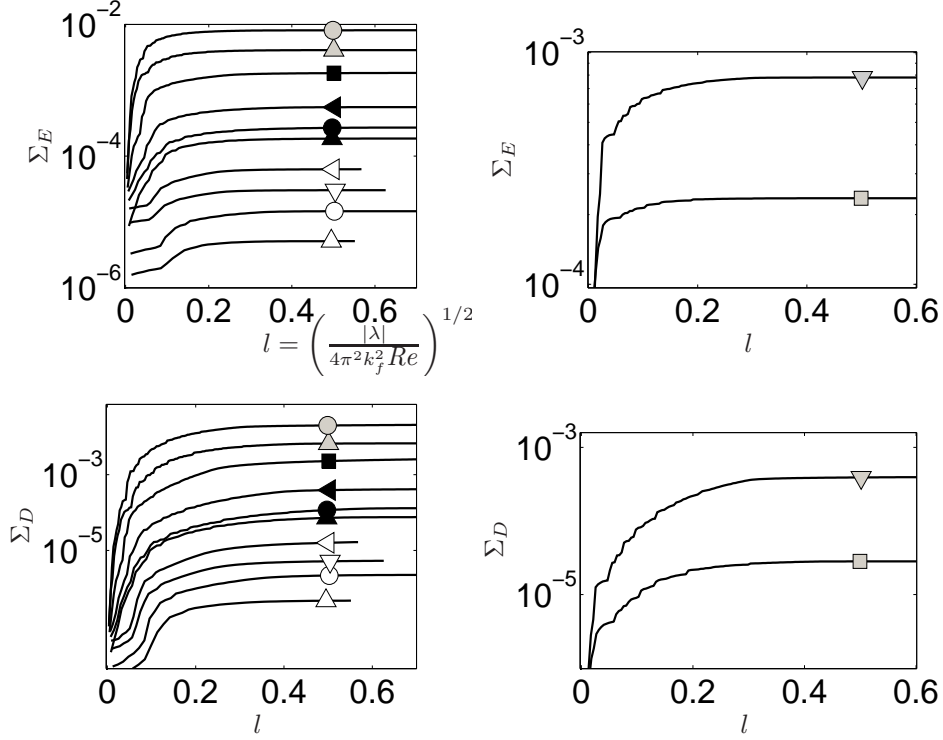


Figure 7: Energy $\Sigma_E(l)$ (*top*) and dissipation $\Sigma_D(l)$ (*bottom*) contained in the subspace $\{\lambda, |\lambda| < 4\pi^2 l^2 Re\}$ vs. l . The symbols are those from table 1 and placed at $l = 0.5$. *Left*: two-dimensional forcing, *right*: three-dimensional forcing.

hand, may fall outside this region and calculations at the corresponding resolution may thus fail to capture noticeable fractions of the total energy and dissipation. On these grounds we shall finally propose the following scaling for λ^{\max} :

$$\frac{\sqrt{|\lambda^{\max}|}}{2\pi k_f} \simeq 0.5 Re^{1/2} \quad (17)$$

The values of k_{\perp}^{\max} and k_z^{\max} can be directly deduced from that of λ^{\max} through (13) to quantify the scalings from Pothérat & Alboussière (2003) as:

$$\frac{k_z^{\max}}{k_f} \simeq 0.8 k_f \frac{Re}{Ha_{\text{opt}}} \quad \frac{k_{\perp}^{\max}}{k_f} \simeq 0.5 Re^{1/2}. \quad (18)$$

Also, the values of λ^{\max} can be expressed as a function of G , which is known *a priori*, unlike Re . Denoting $G_f = \|\mathbf{f}\|_{2f} / (\nu^2 L_f^{3/2})$, where $\|\cdot\|_{2f}$ represents the L_2 norm for a domain of volume $L_f^3 = (L/k_f)^3$, the corresponding graph, on figure 8, suggests the scaling:

$$\frac{\sqrt{|\lambda^{\max}|}}{2\pi k_f} \simeq 0.47 G_f^{0.20}. \quad (19)$$

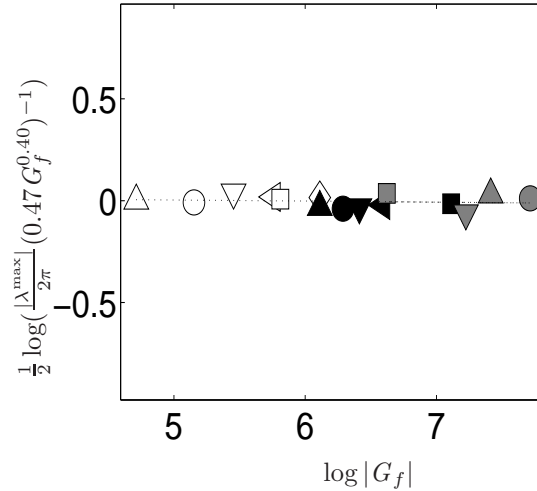


Figure 8: Scaling law for the small scales expressed as a function of G . The symbols correspond to cases from table 1.

Finally, beyond the identification of λ^{\max} , λ -based spectra from figure 5 and 6 exhibit an interesting feature, as a remarkable steep tail is present in both energy and dissipation λ -spectra at high values of λ . In all cases, it starts when λ reaches the value of the eigenvalue $\lambda_J = -Ha_{\text{opt}}^{1/2}$ of the first mode with a wavevector orthogonal to \mathbf{B} . Since $S \gtrsim 1$ in all our calculations, such modes, of the form $((0, k_{\perp}))$, are located outside the Joule cone and therefore strongly suppressed by Joule dissipation. This explains why they carry very little energy.

3.4 Practical use of the scaling laws

The results of the present section now allow us to put forward a simple procedure to resolve three-dimensional MHD flows in periodic domains: firstly, L_{opt} and L_{int} can be calculated at every time step as the numerical simulation progresses (as is already usual for L_{int}). When $S \gtrsim 1$, (17) or (18) then provide criteria for the resolution necessary to represent a three-dimensional MHD flow completely.

When $S < 1$, the flow becomes progressively more isotropic and so does the set of least dissipative modes. Accordingly, the resolution required to fully resolve the flow becomes higher than that predicted by scalings (17) or (18). In this case, L_{int} and L_{opt} are still determined "on the fly" but the usual Kolmogorov criterion must be used instead of (17) or (18).

When $S \gg 1$, the flow can be either two or three-dimensional, which poses an important question about the ability of the least dissipative modes to represent the flow accurately: on the one hand, when λ^{\max} exceeds a value that depends on Ha only, a first three-dimensional mode appears in the set of least dissipative modes, independently of the behaviour of the flow itself. When G is increased from 0, on the other hand, a first three-dimensional physical mode appears in the flow at the actual transition between two- and three-dimensionality, independently of the method used to calculate it. We shall examine in the next section whether both coincide. This will tell us whether the least dissipative modes can be used for the simulation of MHD turbulence, regardless of whether it is two- or three-dimensional.

4 Least dissipative modes at the transition between two-dimensional and three-dimensional turbulence

4.1 Two- vs. three-dimensional sets of least dissipative modes

We now focus on the question of how to calculate flows using the least dissipative modes at the transition between two- and three-dimensional MHD turbulence. The set of least dissipative modes can either contain only two-dimensional modes or both two or three-dimensional modes, depending on the value of λ^{\max} . A transition between these two types of sets therefore occurs at a value $\lambda^{\max} = \lambda^{3D}$ for which the curve $\lambda = \lambda^{\max}$ encloses at least one mode with $k_z \geq 1$ (bold dashed line in Figure 1(d)). According to our previous work (Poth erat & Alboussi ere (2003)) and in the present notations, the first three-dimensional mode in this sense is associated to the eigenvalue

$$|\lambda^{3D}| = 2 \frac{Ha_{\text{opt}}}{2\pi}, \quad (20)$$

and the modulus of the corresponding wavevector in the plane across the magnetic field lines is:

$$|\mathbf{k}_{\perp}^{3D}| = \sqrt{\frac{Ha_{\text{opt}}}{2\pi} - 1}. \quad (21)$$

It is important to notice that although a flow represented by a set comprising three-dimensional modes is potentially three-dimensional, it isn't *necessarily* three-dimensional. Instead it can be either two-dimensional or in a state of intermittency between the two states, as in Zikanov & Thess (1998), if the coefficients of the three-dimensional modes in expansion (10) are 0 or intermittently become 0. This behaviour is determined by the flow dynamics, independently of the basis chosen to represent it (provided the flow is correctly resolved, obviously.). We shall now compare the first least dissipative three-dimensional mode to the first three-dimensional mode that appears in the flow.

4.2 Numerical procedure

We use the same numerical solver as that described in section 3.1 and also the same type of two-dimensional forcing \mathbf{f}_{2D} (14). On the top of previous calculations initialised with the fluid at rest, we now perform two additional series of calculations, at $Ha_0 = 80$ and $Ha_0 = 400$ respectively, as follows: we start with fixed Ha_0 , low G and the fluid initially at rest. We look for a statistically steady two-dimensional solution and let it reach a well developed, turbulent state (after a time of the order of $100 - 200S_0$, or dimensionally, $100-200$ Joule times $\tau_j = \rho/(\sigma B^2)$). With this latter state as the initial condition, we perform the next calculation by increasing the Grashof number by 15%, and repeat the procedure until three-dimensionality appears.

In all simulations the numerical resolutions $n_x \times n_y \times n_z$ are chosen as the smallest powers of 2 such that the resolution domain encloses the $\lambda = 1.5\lambda^{\max}$ curve and satisfies $k_{\perp}^{\max} \geq 1.2k_K = 1.2G^{1/3}(1 + \log G)^{1/6}$. This way, the flow is well resolved whether in a state of two-dimensional turbulence or in a state of three-dimensional MHD turbulence. Since L_{opt} cannot be determined in two-dimensional flows but varies little for a given Ha , we take the approximate values $L_{\text{opt}}(Ha_0 = 80) = 24$ and $L_{\text{opt}}(Ha_0 = 400) = 55$, (see figure 3).

4.3 Measure of three-dimensionality

In order to track three-dimensionality near the transition, we define two quantities to characterise it. The first one expresses how physical quantities depend on z , so we shall call it *morphological*

three-dimensionality and define it as

$$\alpha_{3D} = \left(\int_0^L (f(z) - 1)^2 dz \right)^{1/2}, \quad (22)$$

where $f(z)$ expresses the ratio between the two and three-dimensional parts of the RMS velocity fluctuations in the plane $z = \text{const}$:

$$f(z) = \frac{L_0 \int_{\Omega_{z'=z}} (\langle (\mathbf{u}'(x, y, z'))^2 \rangle_t)^{1/2} dx dy}{\int_{\Omega} (\langle (\mathbf{u}'(\mathbf{x}, \mathbf{y}, \mathbf{z}))^2 \rangle_t)^{1/2} dx dy dz}. \quad (23)$$

Here, $\langle \cdot \rangle_t$ denotes averaging with respect to time and $\mathbf{u}' = \mathbf{u} - \langle \mathbf{u} \rangle_t$ is the local velocity fluctuation. α_{3D} gives a global measure of *morphological* three-dimensionality as it expresses an average ratio of the three-dimensional to the two-dimensional part of the velocity fluctuations.

The second type of three-dimensionality is expressed as the ratio of the energy in the z direction to that in the x and y direction. We shall therefore call it *kinematic* three-dimensionality:

$$\beta_{3D} = \left(\frac{E_z}{E_{\perp}} \right)^{1/2} = \left(\frac{\sum_{\mathbf{k}} w^2(\mathbf{k})}{\sum_{\mathbf{k}} (u^2(\mathbf{k}) + v^2(\mathbf{k}))} \right)^{1/2}. \quad (24)$$

In theory, there is no reason for the first appearance (in the sense of growing G) of these types of three-dimensionality not to take place in vortices of distinct wavelength, which we shall therefore name $k_{\perp}^{3D\alpha}$ and $k_{\perp}^{3D\beta}$ respectively.

4.4 First three-dimensional modes and relevance of the least dissipative modes to transitional flows

On the cases initialised with the fluid at rest, we find that both α_{3D} and β_{3D} jump to finite values at the same value of the forcing $G^{3D}(Ha_{\text{opt}})$. By contrast, when the forcing is increased progressively, morphological three-dimensionality appears at a lower critical value of G than dynamical three-dimensionality. We have identified $k_{\perp}^{3D\alpha}$ and $k_{\perp}^{3D\beta}$ by calculating the quantities $E_{\perp}^{\Sigma\alpha}(k_{\perp}) = \sum_{k_z \geq 1} E_{\perp}(k_{\perp}, k_z)$ and $E_{\perp}^{\Sigma\beta}(k_{\perp}) = \sum_{k_z > 0} E_z(k_{\perp}, k_z)$ respectively. Both are plotted on figure 9 for the first value of the forcing where three-dimensionality was observed. These quantities indeed remain at noise level for two-dimensional flows. When morphological (*resp.* kinematic) three-dimensionality appears, several peaks rise in the profile $E_{\perp}^{\Sigma\alpha}(k_{\perp})$ (*resp.* $E_{\perp}^{\Sigma\beta}(k_{\perp})$) at $k_{\perp} = k_{\perp}^{3D\alpha}$ (*resp.* $k_{\perp} = k_{\perp}^{3D\beta}$). Further peaks also appear around $k_{\perp}^{3D\alpha}$ and $k_{\perp}^{3D\beta}$. This is due to the fact that three-dimensionality can only be detected in slightly supercritical regime. Furthermore, since the maximum of the iso- λ curve in (k_{\perp}, k_z) is not only very ‘‘flat’’ but can also be located at a non-integer value of k_{\perp} , several peaks are expected to rise around the maximum. This is all the more true at high Ha . Keeping this in mind, one still sees that at the lowest forcings where either morphological or kinematic three-dimensionality were detected, both appeared in columnar vortices of approximately the same wavelength $k_{\perp}^{3D\alpha} \simeq k_{\perp}^{3D\beta}$. Importantly, this value is consistent with the theoretical estimate (21) for k_{\perp}^{3D} , albeit a little smaller in the case $Ha_0 = 400$. On the top of the iso- λ curve being very flat at $Ha_0 = 400$, this shift towards larger scales can be explained by the fact that the higher Ha , the higher the value of G at which three-dimensionality appears, and the higher the turbulence intensity when this happens. In two-dimensional turbulence, inertial transfer increases the energy of the large scales, that are therefore more prone to

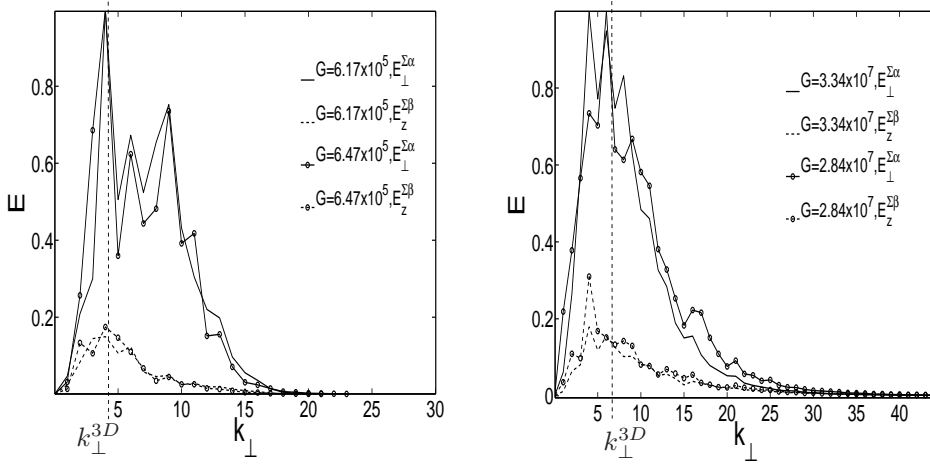


Figure 9: Profiles of $E_{\perp}^{\Sigma\alpha}(k_{\perp})$ and $E_z^{\Sigma\beta}(k_{\perp})$ for $Ha_0 = 80$ (left) and $Ha_0 = 400$ (right): the corresponding flows are weakly three-dimensional. Curves marked with 'o' symbols indicate cases initialised in a stabilised state at slightly lower forcing while curves without them correspond to flows initialised at rest. The vertical dashed lines mark the theoretical values of k_{\perp}^{3D} given by (21).

exhibit instabilities leading to the appearance of three-dimensionality. Among the least dissipative modes that dissipate energy at about the same rate, this favours those with the larger scales, over the strictly least dissipative one predicted by (21).

Importantly, one sees on figure 9 that $k_{\perp}^{3D\alpha} \simeq k_{\perp}^{3D\beta} \simeq k_{\perp}^{3D}$ is independent of the flow's initial conditions, even though α_{3D} and β_{3D} aren't. In other words, even in cases where morphological and dynamical three-dimensionality appear successively (in the sense of growing G) they do so in vortices of the same transverse wavelength (21). This implies that one can use the set of least dissipative modes together with scalings (17) or (18) in order to determine *a priori* the exact set of modes required to resolve both transitional and three-dimensional flows completely, provided L_{opt} is known (It can be obtained from the calculation of a three-dimensional flow at the same value of Ha_0 , for instance.). For flows that lay at the transition between two- and three-dimensionality, a slight over-resolution is advisable that will absorb the peaks of three-dimensionality that appear around $k_{\perp}^{3D} \simeq k_{\perp}^{3D\alpha} \simeq k_{\perp}^{3D\beta}$.

It is quite remarkable that for the forcing (and the forcing scale) we have chosen, k_{\perp}^{3D} follows (21) rather well. Just how universal this behaviour is, however, remains to be clarified. For a sufficiently turbulent two-dimensional flow forced at $k_f > k_{\perp}^{3D}$, the inverse energy cascade can be expected to transfer energy back to k_{\perp}^{3D} where three-dimensional vortices would form. More generally, our recent experiments on MHD turbulence in cubic box have shown that the appearance of three-dimensionality was governed by a subtle interplay between inertia and the Lorentz force at the scale of each structure (Klein & Pothérat (2010)). The former is determined on the one hand by the forcing, which arbitrarily injects energy in the flow and, on the other hand, by the turbulent redistribution of energy amongst structures. Flows where turbulence is absent or too weak to sufficiently erase the non-universal trace of the forcing, therefore don't exhibit the ideal behaviour predicted by (21). This was spectacularly illustrated in our experiment where at low Ha and low Re , the destabilisation of a periodic array of columnar vortices led to remarkable steady

three-dimensional Y-shaped vortices.

5 Conclusions

In this article, we have shown that DNS of Low- Rm MHD turbulence in a three-dimensional periodic domain could be achieved by using the sequence of least dissipative eigenmodes from the dissipation operator instead of the traditional Fourier basis. Not only is this technique far more cost effective at fully resolving the flow without modelling, but it also enlightens some of its properties that don't appear otherwise. Indeed, the iso-energy lines follow the lines of constant linear decay rate λ well in regions of the spectral space that are not directly influenced by the forcing. Furthermore, energy and dissipation spectra expressed in terms of the eigenvalue λ associated to these modes instead of k , exhibit a clear cutoff that identifies modes located inside the Joule cone, and therefore strongly suppressed by Joule dissipation. Most importantly, analysing this spectra for $S \gtrsim 1$ allowed us to derive laws that play the role of Kolmogorov laws, of determining the small scales in MHD turbulence: $\sqrt{|\lambda^{\max}|}/(2\pi k_f) \simeq 0.5 Re^{1/2}$ or $\sqrt{|\lambda^{\max}|}/(2\pi k_f) \simeq 0.47 G^{0.20}$. Finally, MHD flows in a periodic domain can be resolved as follows: L_{opt} and L_{int} can be obtained on the fly, by minimising functional Σ_{E_λ} at every time step (see section 3.2). The discrete sequence of values of λ then follows from (9), and ultimately, the small scales are obtained using our new scalings (17) if $S_{\text{opt}} \gtrsim 1$, or the Kolmogorov laws if $S < 1$.

In the last part of this work, we also showed that the set of least dissipative modes encompassed the modes that first exhibit three-dimensionality when the forcing was increased from either zero or from that of a two-dimensional flow. This proves that the set of least dissipative modes is also suitable for the resolution of transitional flows, and not only for three-dimensional flows. On the top of this, for two-dimensional flows, that occur in the limit of large S , the Lorentz force vanishes so the set of least dissipative modes coincides with the usual set of two-dimensional Fourier modes. They can therefore be used in conjunction with Kraichnan's law for the size of the smallest scales $|\lambda^{\max}|^{1/2}/(2\pi) \simeq G^{1/3}$. The least dissipative modes can therefore be used to calculate MHD flows in a periodic box for all values of S .

Finally, we wish to underline the large potential field of application of the method presented in this work. The initial idea was to use a basis of modes that already incorporates the main constitutive structures of the flow, so as to save the costs of having to reconstruct them using elements of a less suited basis. In the present case, the basis of least dissipative modes readily rendered the anisotropic properties of MHD turbulence. Using this basis therefore reduced the cost of DNS by confining the spectral domain of resolution to that strictly relevant to the flow dynamics. This procedure can clearly be extended to MHD and non-MHD problems with more complex boundary conditions. We have recently shown that the orthogonal set of least dissipative modes in a channel flow with transverse magnetic field were exponential functions that incorporated the profile of the very thin Hartmann boundary layers which arise along the walls (Dymkou & Poth erat (2009)). Currently, channel flow DNS are limited to Ha below a few hundred because of the computational cost involved in meshing these layers. Using the least dissipative modes for this problem not only brings the same benefits as in the periodic case studied in the present work, but it also eliminates the difficulty posed by the Hartmann layers as they do not have to be reconstructed nor meshed. As a spectacular consequence, the computational cost of DNS based on these modes decreases with Ha instead of increasing as in current methods based on Tchebychev Polynomials. Using the least dissipative modes is therefore not only beneficial to the simulation of turbulent flows but also potentially to all flows where the reconstruction of anisotropic structures with unsuited elements incurs computational costs far beyond those strictly required by the dynamics.

The authors would like to express their gratitude to the Deutsche Forschungsgemeinschaft for their financial support under grant P01210/1-1. Part of the work presented here was performed during the MHD summer school organised by the Statistical and Plasma Physics department at the Universit e Libre de Bruxelles in 2007. The bulk of the numerical computations was performed on the computational facilities of the Applied Mathematics Research Centre at Coventry University.

References

- ALEMANY, A., MOREAU, R., SULEM, P. & FRISH, U. 1979 Influence of an external magnetic field on homogeneous MHD turbulence. *J. Mec.* **18:2**, 277–313.
- CANUTO, C., HUSSAINI, M. Y., QUARTERONI, A. & ZANG, T. A. 2006 *Spectral Methods: Fundamentals in Single Domains*. Springer-Verlag.
- CONSTANTIN, P., FOIAS, C., MANNLEY, O.P. & TEMAM, R. 1985 determining modes and fractal dimension of turbulent flows. *J. Fluid. Mech.* **150**, 427–440.
- DAVIDSON, P.A. 2004 *Turbulence: An Introduction for Scientists and Engineers*. Oxford University Press.
- DAVIDSON, P. A. 1997 The role of angular momentum in the magnetic damping of turbulence. *J. Fluid Mech.* **336**, 123–150.
- DELANNOY, Y., PASCAL, B., ALBOUSSI ERE, T., USPENSKI, V. & MOREAU, R. 1999 Quasi-two-dimensional turbulence in MHD shear flows: The matur experiment and simulations. In *Transfer Phenomena and Electroconducting Flows* (ed. A. Alemany et al.). Kluwer.
- DOERING, C.R. & GIBBONS, J.D. 1995 *Applied analysis of the Navier-Stokes equation*. Cambridge University Press.
- DYMKOU, V. & POTH ERAT, A. 2009 Spectral methods based on the least dissipative modes for wall-bounded MHD flows. *J. Theor. Comp. Fluid Dyn.* **23** (6), 535–555.
- FOIAS, C., MANLEY, O., ROSA, R. & TEMAM, R. 2001 *Navier-Stokes Equations and Turbulence*. Cambridge University Press.
- FRISCH, U. 1995 *Turbulence, The legacy of A.N. Kolmogorov*. Cambridge University Press.
- KLEIN, R. & POTH ERAT, A. 2010 Appearance of three-dimensionality in wall-bounded MHD flows. *Phys. Rev. Lett* **104** (3), 034502.
- KLEIN, R., POTH ERAT, A. & ALFERJONOK, A. 2009 Experiment on an electrically driven, confined vortex pair. *Phys. Rev. E* **79** (1), 016304 (14 pages).
- KNAEPEN, B. & MOIN, P. 2004 Large-eddy simulation of conductive flows at low magnetic Reynolds number. *Phys. Fluids* **16:5**, 1255–1261.
- KOLMOGOROV, A.N. 1941 Local structure of turbulence in an incompressible fluid at very high Reynolds numbers. *Dokladi Akademii Nauk SSSR* **30**, 299–303.
- KRAICHMAN, R.H. 1967 Inertial ranges in two-dimensional turbulence. *Phys. Fluids* **10**, 1417.
- MININNI, P. D., ALEXAKIS, A. & POUQUET, A. 2006 Large-scale flow effects, energy transfer, and self-similarity on turbulence. *Phys. Rev. E* **74**, 016303.
- MOFFATT, H.K. 1967 On the suppression of turbulence by a uniform magnetic field. *J. Fluid Mech.* **28**, 571–592.

- MOREAU, R. 1990 Magnetohydrodynamics. Kluwer Academic Publisher.
- NAKAUCHI, N., OSHIMA, H. & SAITO, Y. 1992 Two-dimensionality in low-magnetic Reynolds number magnetohydrodynamic turbulence subjected to a uniform external magnetic field and randomly stirred two-dimensional force. *Phys. Fluids A* **12** (4), 2906–2914.
- OHKITANI, J. 1989 Log corrected energy spectrum and attractor dimension in two-dimensional turbulence. *Phys. Fluids A* **1** (3), 451–452.
- ORSZAG, G. S. & PATTERSON, S. A. 1971 Spectral calculations of isotropic turbulence: Efficient removal of aliasing interaction. *Phys. Fluids* (14), 2538–2541.
- POTH ERAT, A. & ALBOUSSI ERE, T. 2003 Small scales and anisotropy in low-Rm magnetohydrodynamic turbulence. *Phys. Fluids* **15:10**, 3170–3180.
- POTH ERAT, A. & ALBOUSSI ERE, T. 2006 Bounds on the attractor dimension for low-Rm wall bound MHD turbulence. *Phys. Fluids* **18:12**, 125102.
- POTH ERAT, A., SOMMERIA, J. & MOREAU, R. 2000 An effective two-dimensional model for MHD flows with transverse magnetic field. *J. Fluid Mech.* **424**, 75–100.
- ROBERTS, P.H. 1967 *Introduction to Magnetohydrodynamics*. Longmans, London.
- ROGALLO, R.S. 1981 Numerical experiments in homogeneous turbulence. National Aeronautics and Space Administration. Ames Research Center, Moffett Field, CA.
- SCHUMANN, U. 1976 Numerical simulation of the transition from three- to two-dimensional turbulence under a uniform magnetic field. *J. Fluid Mech.* **35**, 31–58.
- SOMMERIA, J. 1986 Experimental study of the two-dimensional inverse energy cascade in a square box. *J. Fluid Mech.* **170:139**.
- SOMMERIA, J. 1988 Electrically driven vortices in a strong magnetic field. *J. Fluid Mech.* **189**, 553–569.
- SOMMERIA, J. & MOREAU, R. 1982 Why, how and when, MHD turbulence becomes two-dimensional. *J. Fluid Mech.* **118:507**.
- THESS, A. & ZIKANOV, O. 2007 Transition from two-dimensional to three-dimensional magnetohydrodynamic turbulence. *J. Fluid Mech.* **579**, 383–412.
- VOROBEV, A, ZIKANOV, O., DAVIDSON, P. A. & KNAEPEN, B. 2005 Anisotropy of magnetohydrodynamic turbulence at low magnetic Reynolds number. *Phys. Fluids* (17), 125105.
- WILLIAMSON, J.H. 1980 Low-storage Runge-Kutta schemes. *J. Comp. Phys.* **35**, 48–56.
- ZIKANOV, O. & THESS, A. 1998 Direct numerical simulation of forced MHD turbulence at low magnetic Reynolds number. *J. Fluid Mech.* **358**, 299–333.